Ascertaining higher MRR at chatter free milling using spline-based local mean decomposition and artificial neural network based hybrid approach

Rohit Mishra[1] and Bhagat Singh[1,*]

[1]Mechanical Engineering Department, Jaypee University of Engineering and Technology, Guna (M.P.), India, 473226

[*]Corresponding author's E-mail : dr.bhagatsinghjuet@gmail.com,

First author's E-mail : rohitmishra2288@gmail.com,

Abstract: Chatter is a type of self-induced vibration that reflects fluctuations in both frequency and energy dispersion during the milling process, inevitably resulting in substandard part quality and diminished material removal rates. It is essential to employ a robust chatter detection method to anticipate its emergence in the early stages. This study introduces an efficient Product Function (PF) based multi-mode signal processing technique, specifically the spline-based local mean decomposition (SBLMD). This method is applied to decompose sound signals acquired through experimentation into a series of effective PF's. Subsequently, selected PFs are employed to reconstruct a new chatter signal that is information-rich. Additionally, prediction models based on Artificial Neural Networks (ANN) are established to predict Chatter Indicator (CI) and Material Removal Rate (MRR) using three different activation algorithms: Tan Sigmoid (TANSIG), Log Sigmoid (LOGSIG), and Purely Linear (PURELIN). Statistical comparisons have been conducted in order to obtain the optimal activation algorithm and found out that data set trained with LOGSIG gives minimal error. Moreover, an optimal range of input parameters has been selected pertaining to minimum chatter and maximum MRR. Confirmation tests on the obtained set of parameters have been carried out in order to analyse and authenticate the proposed technique.

Keywords: Signal processing; Chatter Indicator; SBLMD; LM-BPNN; MRR

1. Introduction

Chatter has always been a serious obstacle to manufacturing industries. Chatter may lead to many detrimental consequences such as; poor surface finish, less tolerance, tool wear and breakage, material wastage and many more. From the aforementioned negative consequences of chatter, it can be inferred that the chatter directly affects stability and productivity of the machining system [1]. The identification and mitigation of chatter represent ongoing priorities for machinists. Effectively managing chatter at its incipient stage is crucial to preventing damage to both part quality and Material Removal Rate (MRR). In recent years,

researchers have introduced numerous process-based approaches aimed at early detection and recognition of chatter. These approaches not only enhance machining efficiency but also contribute to advancements in manufacturing precision and productivity. Ongoing research in this area is essential for the continual improvement of machining technology in alignment with evolving industry standards.

A schematic of the online chatter detection process based on sensors is depicted in Figure 1. In the initial phase, raw signals are gathered utilizing a signal acquisition system. Following this, the second phase involves three operations: signal processing, signal transformation, and feature extraction. The concluding step employs a soft computing method to create a classifier for the prediction of chatter.

In sensor based online chatter detection methods, data acquisition (which represents the dynamics of the cutting system) is the first stage. In order to acquire the data from the cutting system, sensors which are primarily used are accelerometers (acceleration signal) [2], dynamometers (force signal) [3] and microphones (sound signal) [4,5]. Cuka et al. [4] utilized a multi-sensor approach to construct a tool condition monitoring system, incorporating a dynamometer, an accelerometer, a microphone, and a current sensor. Their investigation revealed challenges in filtering the accelerometer signal, leading to potential errors. The study also concluded that sound signals obtained through a microphone produced superior and more reliable results, attributed to their low error ratio, minimal overlapping effects, and higher sampling rates.

The second step i.e., signal processing, involves the manipulation and analysis of signals generated during milling processes to detect and address unstable vibrations. Signal processing techniques, such as filtering, transformation, and feature extraction, play a crucial role in identifying and isolating chatter signals from the overall machining noise. By implementing advanced signal processing methods, such as Short-Time Fourier Transform (STFT) [6], Continuous Wavelet Transform (CWT) [7,8], Synchronous Compression Wavelet (SCWT) [9], Wigner-Ville Distribution (WVD) [10], Empirical Mode Decomposition (EMD) [11], Empirical Wavelet Transform (EWT) [12], Variational Mode Decomposition (VMD) [13,14], and many others, machinists can gain insights into the incipient stages of chatter, allowing for timely intervention and mitigation strategies to ensure smoother and more precise machining operations [15].

However, all the above stated signal processing methods have its own set of drawbacks, such as the end effect, mode aliasing, noise sensitivity, and sampling issues with EMD [16]. Mode numbers must be specified in advance for the VMD approach. Because establishing the mode numbers needs the operator's experience and expertise, VMD's adaptability is severely constrained [17]. EWT has their own limitation such as leading to an improper segmentation in the frequency domain, which is reported by researchers in their work [17]. Smith [18] suggested a novel self-adaptive signal processing technology called LMD to meet the challenge of EMD. In order to obtain the local envelope estimate and local mean functions, Moving average method has been invoked in LMD. Recently, Mishra et al. used the local mean decomposition based on cubic spline function technique to detect tool chatter in the milling process using statistical indicators [19]. By using SBLMD, any non-linear and non-stationary signal (chatter signal) can be decomposed in the Product Functions (PF's). PF's are the set of functions of any chatter signal, which are obtained by the product of amplitude modulated (AM) signal and a frequency modulated (FM) signal.

Following the extraction of chatter features, diverse models for predicting chatter was developed using various techniques, including Artificial Neural Networks (ANN)[20,21], fuzzy logic [22], Support Vector Machines (SVM) [23], Self-Organising Maps (SOM) [24], Response Surface Methodology (RSM) [25] and other classification models [26]. It's noteworthy, however, that there is a gap in the existing literature concerning the consideration of chatter in conjunction with Material Removal Rate (MRR). Both MRR and chatter are intertwined with machining process variables, yet previous studies have often overlooked the impact of the table feed rate on MRR during chatter investigations. In the contemporary manufacturing landscape, industries are actively exploring methods to enhance productivity while ensuring superior surface quality in machined products. Since productivity correlates with MRR and chatter intensity adversely affects surface finish, these two aspects cannot be disregarded. This gap in understanding prompted the current research. Recently, the neural network approach has gained traction in various engineering fields [27–29]. However, there remains a challenge in selecting the appropriate activation algorithm for ANN modelling to avoid over- and underfitting, emphasizing the need for a robust strategy in this regard.

2. Chatter signal simulation model

The simulation of a real-time operational chatter signal has been accomplished by employing a spring-mass model [30] for the milling mechanism, illustrated in Figure 2. This model takes

into account the intricacies of milling cutters, each equipped with multiple teeth that engage intermittently with the workpiece. It is assumed in this model that the milling cutter has a specific number of teeth and a zero-helix angle. As the machining process unfolds, cutting forces act upon the milling cutter, causing dynamic displacements along both the feed (X) and normal (Y) directions. These cutting-induced forces play a crucial role in exciting the structure, leading to vibrations represented as x and y in their respective directions.

Before delving into the force components, it is crucial to express the general equation of motion governing the system in both the feed (X) and normal (Y) directions, encapsulated in Equation 1. This equation forms the basis for understanding the dynamic behavior of the milling mechanism and provides a foundation for further analysis and exploration of how the system responds to cutting forces.

$$m_x \ddot{x}(t) + b_x \dot{x}(t) + k_x x(t) = F_x(t)$$
$$m_y \ddot{y}(t) + b_y \dot{y}(t) + k_y y(t) = F_y(t)$$

…….. (1)

The assessment was carried out with a randomly assigned rotating tooth number, denoted as "k". The spindle rotates at an angular speed (Ω) in radians per second. When the arbitrary tooth "k" is positioned at the angular immersion ($\theta_k(t) = \Omega t$) measured clockwise from the y-axis, the dynamic chip thickness in the radial direction is shaped by vibrations occurring during both the current and preceding tooth periods is given by Equation 2;

$$\begin{bmatrix} \Delta x(t,T) = \left[x_{tool}(t) - x_{work-piece}(t) \right] - \left[x_{tool}(T-t) - x_{work-piece}(T-t) \right], \\ \Delta y(t,T) = \left[y_{tool}(t) - y_{work-piece}(t) \right] - \left[y_{tool}(T-t) - y_{work-piece}(T-t) \right] \end{bmatrix} \text{as}$$

$$s(\theta_k) = \left[f_t \sin\theta_k + (v_{k,0} - v_k) \right] u(\theta_k)$$

…….. (2)

Where, '$f_t \sin \theta_k$' is the static part of the resulting chip thickness and $(v_{k,0}, v_k)$ are the dynamic displacements of the cutter at the previous and present tooth periods, respectively. $u(\theta_k)$ is a unit step function that determines whether the tooth is in or out of cut, is given by Equation 3

$$\left. \begin{matrix} u(\theta_k) = 1 \leftarrow \theta_{st} < \theta_k < \theta_{ex}, \\ u(\theta_k) = 1 \leftarrow \theta_k < \theta_{st} \ or \ \theta_k > \theta_{ex} \end{matrix} \right\},$$

…….. (3)

Where, θ_{st} and θ_{ex} are the entry and exit immersion angles of the cutter to and from the cut, respectively. Since, Static chip thickness i.e., '$f_t \sin \theta_k$' does not contribute in the regeneration

4

mechanism and so it has been removed from the dynamic chip thickness equation. Therefore, modified dynamic chip thickness equation can be represented as Equation 4;

$$s(\theta_k) = \left[v_{k,0} - v_k \right] u(\theta_k)$$ ……….. (4)

Now, after resolving the displacement of the cutter in x and y direction at given angle θ_k , $'v_{k,0}'$ can be written as $x_{t-T} \sin\theta_k(t) + y_{t-T} \cos\theta_k(t)$ and $'v_k'$ can be written as $x_t \sin\theta_k(t) + y_t \cos\theta_k(t)$.

Where, 't' is the time and 'T' is the time period of the cutter revolution.

Now, placing these values in Equation 4, we get

$$s(\theta_k) = \left[(x_{t-T} \sin\theta_k(t) + y_{t-T} \cos\theta_k(t)) - (x_t \sin\theta_k(t) + y_t \cos\theta_k(t)) \right] u(\theta_k)$$ ……….. (5)

After rearranging the displacement of cutter in x and y direction, Equation 5 can be presented as Equation 6;

$$s(\theta_k) = \left[(x_{t-T} - x_t) \sin\theta_k(t) + (y_{t-T} - y_t) \cos\theta_k(t) \right] u(\theta_k)$$ ……….. (6)

Where, $(x_{t-T} - x_t) = \Delta x$ and $(y_{t-T} - y_t) = \Delta y$ are the current displacement of the cutter in x and y direction with respect to the previous cutter position. Therefore, modified dynamic chip thickness equation can be presented as Equation 7;

$$s(\theta_k) = \left[\Delta x \sin\theta_k + \Delta y \cos\theta_k \right] u(\theta_k)$$ …….. (7)

The cutting forces that happen tangentially and radially on tooth "k" increase in line with the axial depth of cut (b) and the chip thickness (s). It can be expressed as Equation 8:

$$F_{tk} = K_k b s(\theta_k), \qquad F_{rk} = K_r F_{tk},$$ …….. (8)

By rearranging the radial and tangential forces in the x and y directions and taking the Fourier transform, it can be expressed as Equation 9;

$$\mathcal{F}\{F(t)\} = \frac{1}{2} b K_t \mathcal{F}\left[D(t) \right] * \mathcal{F}[\{\Delta(t)\}]$$

$$\{F(\omega)\} = \frac{1}{2} b K_t \{[D(\omega)] * \{\Delta(\omega)\}\}.$$ …….. (9)

By taking the Dirac delta function and Fourier transformation, directional coefficient matrix can be written as value of harmonic is changing from $r = 0, \pm 1$ as Equation 10;

$$[D(t)] = \sum_{r=-1}^{+1} [D_r] \, e^{ir\omega_T t}$$ .... (10)

Authors construct a simulated signal by adding white Gaussian noise to an original frequency set of 41, 80, 106, 141, and 350 Hz, aiming to mimic a real chatter signal. Developed simulated signal is presented in Figure 3(a). A real-time simulated signal was then created with N (number of teeth) set at 4, and cutting coefficients K_t and K_r are 796 N/mm^2 and 0.212, respectively. To identify the frequency peaks of the simulated signal, Fast Fourier Transform (FFT) was applied, and the results are shown in Figure 3(b). Notably, direct FFT on the simulated signal with white Gaussian noise is discouraged for effectively visualizing its frequency peaks, as evident from Figure 3(b).

3. Proposed signal processing techniques

3.1. Spline Based Local Mean Decomposition (SBLMD)

The data points, $(x_0, y_0), (x_1, y_1) \ldots \ldots (x_n, y_n)$ has been selected for understanding the cubic spline based fitting.

In order to have cubic spline based fitting function $f(x)$ should follow listed conditions:

    i.   Outside the (x_0, x_n) band $f(x)$ must be a polynomial of degree one,

    ii. $f(x)$ must be a polynomial of three degree in the subintervals,

    iii. Differential and double differential of $f(x)$ must be continuous.

Since in each of the subintervals, $f(x)$ is a cubic function then obviously $f''(x)$ is going to be linear.

Taking equally-spaced values of x so that $x_{i+1} - x_i = h$, it can be written as Equation 11

$$f''(x) = \frac{1}{h}[f''(x_i) \times (x_{i+1} - x) + f''(x_{i+1}) \times (x - x_i)]$$ .... (11)

Integrating twice, we have $f(x)$ presented as Equation 12;

$$f(x) = \frac{(x-x_i)(x_{i+1}-x)a_i}{h \times 3!} f''(x_{i+1}) + \frac{(x_{i+1}-x)^2 a_i}{h \times 3!} f''(x_i) + b_i(x-x_i)$$ .... (12)

The constants of integration a_i, b_i are determined by substituting the values of $y = f(x)$ at x_i and x_{i+1}. Thus,

$$a_i = \frac{y_i}{h} - \frac{h}{3!} f''(x_i), b_i = \frac{y_{i+1}}{h} - \frac{h}{3!} f''(x_{i+1})$$

Substituting the values of a_i, b_i and writing $f''(x_i) = M_i$, Equation 12 takes the form Equation 13

$$f(x) = \frac{(x_{i+1} - x)}{h}\left[\left\{\frac{(x_{i+1} - x)^2}{6} - \frac{h^2}{6}\right\}M_i + y_i\right] + \frac{(x - x_i)}{h}\left[\left\{\frac{(x - x_i)^2}{6} - \frac{h^2}{6}\right\}M_{i+1} + y_{i+1}\right]$$

(13)

$$\therefore f'(x) = -\frac{(x_{i+1} - x)^2}{2h}M_i + \frac{(x - x_i)^2}{6h}M_{i+1} - \frac{h}{6}(M_{i+1} - M_i) + \frac{1}{h}(y_{i+1} - y_i)$$

To impose the condition of continuity of $f'(x)$, we get

$$f'(x - \varepsilon) = f'(x + \varepsilon) \text{ as } \varepsilon \to 0$$

$$\therefore \frac{h}{6}(2M_i + M_{i-1}) + \frac{1}{h}(y_i - y_{i-1}) = -\frac{h}{6}(2M_i + M_{i+1}) + \frac{1}{h}(y_{i+1} - y_i)$$

$$M_{i-1} + 4M_i + M_{i+1} = \frac{6}{h^2}(y_{i-1} - 2y_i + y_{i+1}), i = 1.....(n-1)$$

To get the remaining terms, the first derivative values has been used which are known constants. Cubic spline will be obtained after putting the value of M_i in Equation 13.

To get around the limitations of the conventional LMD (C-LMD) method, the aforementioned mathematical details underlying the spline-based interpolation have been used. To obtain the product functions in this method, cubic spline interpolation substitutes the moving average in the traditional LMD with the subsequent steps.

1. Find the signal's local extremes first. Next, link one cubic spline line to all local maxima and another cubic spline line to all local minima. As a result, a top layer $P_{tl}(t)$ and a bottom layer $P_{bl}(t)$ will form.

2. The terms presented in Equation 14 are used to evaluate the local mean function $m_{11}(t)$ and the local envelope estimate function $a_{11}(t)$;

$$m_{11}(t) = \frac{P_{tl}(t) + P_{bl}(t)}{2} \quad a_{11}(t) = \frac{|P_{tl}(t) - P_{bl}(t)|}{2} \quad \text{........ (14)}$$

3. Now, remaining step will be same as in the conventional LMD algorithm as shown in Figure 4.

3.2. Conventional-LMD Processing and Results

In this section, the conventional Local Mean Decomposition (LMD) technique was employed to analyse the simulated chatter signal developed in Section 2. After decomposition, the resulting Product Functions (PFs) are showcased in Figure 5(a). To pinpoint the frequency peaks of the simulated chatter signal, Fast Fourier Transform (FFT) was employed. Specifically, FFT was employed on the first three PFs, revealing the frequency peaks

illustrated in Figure 5(b). It's worth noting that the spectrums of the first PFs lack clarity and do not align with the original frequency peaks. This suggests that conventional LMD may not effectively extract the original frequency peaks.

3.3. SBLMD Processing and Results

The preceding analysis underscores the inadequacy of the conventional LMD method in effectively examining signals that exhibit variations in both time and frequency. In response to this limitation, SBLMD approach is invoked in this section. The decomposed Product Functions (PFs) resulting from SBLMD applied to the simulated chatter signal are visually presented in Figure 6(a). Further insight into the frequency domain of the first three PFs is provided in Figure 6(b). Notably, Figure 6(b) vividly demonstrates that SBLMD adeptly captures the original frequencies inherent in the simulated signals. Consequently, it is unequivocal that the SBLMD approach is highly recommended for the nuanced analysis of signals characterized by concurrent variations in both time and frequency.

4. Acquisition of real milling signal using microphone

Conclusive experiments have been executed on a milling machine with the objective of real-time identification and extraction of tool chatter features. These milling trials, specifically designed for slotted configurations, have been conducted under 27 cutting conditions, outlined comprehensively in Table 1. Notably, in these slotted experiments, the radial depth of cut consistently remained fixed, equivalent to the diameter of the milling cutter (10 mm). The experimentation featured the utilization of a four-tooth High-Speed Steel (HSS) milling cutter. The chosen workpiece material for these trials have been on Aluminium alloy (Al 6061-T6 series), a material widely employed in aviation industries. To provide a visual context, Figure 7 showcases a photograph detailing the experimental setup, offering a glimpse into the practical aspects of the conducted milling experiments. Moreover, One of the acquired milling signal using microphone during experimentation has been shown in Figure 8. Presented real time machining signal is of Experiment No. 4.

Evaluation of responses

This study focuses on the Material Removal Rate (MRR) as its key response variable. MRR is quantified through the application of the relationship outlined in Equation 15, and a visual representation of the MRR results can be found in Figure 9:

$$MRR = \frac{Initial \ weight \ (W_i) \ - \ final \ weight \ (W_f)}{Machining \ time \ (T_m)} \qquad \text{........ (15)}$$

4.1. SBLMD in real milling signals

After validating the effectiveness of SBLMD for simulated signal, now, it has been utlized for processing the real milling signal. Extracted PF's using SBLMD are presnted in Figure 10. Thereafter, in order to sieve out the noisy data from the orginal signal, two important indicators, pearson correlation coefficient (CC) and energy ratio (NER) are adopted and their outcomes for each PF's has been presented in Figure 11. Correlation coefficient is generally adopted to find the interdependency of the retrieved PF's with respect to their original signal using following Equation 16:

$$\Delta(pf, os) = \frac{1}{X-1} \sum_{k=1}^{X} \left(\frac{pf_k - \mu_{pf}}{\sigma_{pf}} \right) \left(\frac{os_k - \mu_{os}}{\sigma_{os}} \right)$$

.... (16)

Where, X = signal data, μ_{pf} and μ_{os} are the mean of individual PF and acquired machining signal, respectively and σ_{pf} and σ_{os} are the standard deviation of individual PF and acquired machining signal, respectively. Whereas, Energy ratio are adopted to calculate the energy content of the individual PF's with respect to the acquired machining signal.

The determination of CC and NER values is conducted under normalized conditions. Analysis of Figure 11 distinctly reveals that the first three PFs carry more significant chatter information. Consequently, to visually enrich the signal with meaningful chatter details, these initial three critical PFs are amalgamated and synthesized.

In order to visualize the frequency peaks of the newly reconstructed chatter rich milling signal, FFT has been utilized and the spectral domain of the signal is presented in Figure 12. By observing the Figure 12, three distinct frequencies can be easily recognized viz. cutter frequency (ω), the multiple of cutter frequency ($2\omega, 3\omega \ldots$) along with chatter frequency (ω_c). Hence, it can be concluded that SBLMD is quite able to extract the chatter features from non-linear and non-stationary signals.

4.2. Determining the Response for the Prediction Model

In this study, two responses, i.e., CI and MRR have been utilized to developed prediction model. Their values and ascertaining methods have been illustrated in the subsequent subsections.

9

4.2.1. Chatter Indicator

To study the impact of milling parameters on chatter, a novel statistical parameter—specifically, the coefficient of variance—has been introduced as a Chatter Indicator (CI) as expressed in Equation 17;

$$CI = \frac{\text{Standard deviation } (\sigma)}{\text{Mean } (\bar{x})} \qquad \dots\dots (17)$$

The CI value correlates directly with the presence of chatter components in the signal. The Chatter Indicator has been computed for each of the 27 experimental runs, and the results are visually presented in Figure 13. Establishing upper and lower thresholds, denoted by red and green lines, respectively, using the 3σ criterion, enables the classification of three domains representing chatter intensity, as depicted in Figure 13. Instances where CI values fall below the green line are considered satisfactory, while those surpassing it are deemed otherwise. This visual representation offers a clear and intuitive understanding of the chatter intensity across different experimental conditions.

4.2.2. MRR

MRR can be emerged as an alternative strategy for refining the prediction model. To enhance the clarity of our findings, MRR have been computed for each of the 27 experimental runs by applying Equation 15. The graphical representation of these calculations is vividly presented in Figure 9, providing a visual insight into the impact of MRR on our predictive model

5. Artificial Neural Network's Structure

In this study, the three layers based ANN model are used as presented in Figure 14. In the developed model, three input milling parameters (CS, TF and ADC) has been used as an input. In hidden layer, 10 neurons have been considered. In output layer, two responses (MRR and CI) have been considered. In this study, model has been trained with LM based training algorithm.

Moreover, in order to assess the effect of activation algorithm on the model, three different activation algorithms has also been considered and is as follows:

1. Tangent sigmoid (TANSIG) = $\dfrac{2}{1+e^{-2z}} - 1$

2. Log sigmoid (LOGSIG) = $\dfrac{1}{1+e^{-z}}$

3. Linear (PURELIN) = z

6. Result and discussion

6.1. Comparison between Activation function

Absolute percentage deviation has been calculated in order to assess the algorithms' propensity for prediction, and it is shown in Table 2. For each algorithm, the final average absolute percentage deviation (AAPD) has been determined.

The average absolute percentage deviation (AAAPD) for MRR and CI are 7.615 % and 4.310 %, respectively, when TANSIG is employed as a training function. MRR and CI for LOGSIG as a training function are 4.250 % and 3.745 %, respectively. AAPD for MRR and CI are 5.938 % and 11.551 %, respectively, when PURELIN is used as a training function. Figures 15 and 16 demonstrate the percentage error for MRR and CI using the TANSIG, LOGSIG, and PURELIN training functions. After analysing all of the potential combinations of the chosen training functions, it can be concluded that LM with LOGSIG is the best combination for predicting the output.

6.2. Effect of milling inputs on responses

A mathematical model was formulated to delve into the intricate influence of specific parameters on two crucial aspects of milling operations: Material Removal Rate (MRR) and Chatter Indicator (CI). The key players shaping the monotonic function of MRR are the table feed rate, axial depth of cut, and radial depth of cut. When these parameters are introduced, MRR exhibits a clear and linear ascent.

Chatter, a disruptive phenomenon during milling, exacts a toll on both surface finish and tool longevity. To optimize the milling process for enhanced MRR, superior surface precision, and prolonged tool life, it becomes imperative to mitigate the impact of Chatter Indicator (CI). This indicator is intricately tied to the interplay of input milling parameters. Visualizing this interaction, the section employs illustrative contour plots, exemplified in Figure 17, to vividly portray the effects of these interplaying factors on both MRR and CI.

In Figures 17 (a) and (d), the charts depict the variations in Material Removal Rate (MRR) and Chatter Indicator (CI) concerning the axial depth of the cutter (ADC) and cutter speed (CS) while maintaining a consistent table feed rate (TF) of 75 mm/min. Transitioning to

Figures 17 (b) and (e), the graphs showcase the deviations in MRR and CI based on the axial depth of the cutter (ADC) and table feed rate (TF), with a steady cutter speed (CS) set at 2000 rpm. Finally, Figures 17 (c) and (f) exhibit the changes in MRR and CI in relation to the table feed rate (TF) and cutter speed (CS), while holding the axial depth of the cutter (ADC) constant at 1.5 mm.

These visual representations employ a distinct colour scheme (red, tangerine, yellow, blue, dark green, and green) to highlight the fluctuations in MRR and CI. The colour spectrum indicates the extent of these variations, with red and green denoting the minimum and maximum values of MRR and CI within the considered range of parameters. This graphical approach provides a clear visual representation of the observed trends without replicating existing content.

The suitable range of MRR (green colour) and CI (green colour) has been estimated after taking into account all six of these figures, as shown in Table 3.

After getting the value of Metal removal rate (MRR) and Chatter Indicator (CI) for three cases (Satisfactory, Medium and Unsatisfactory), a range of milling parameters has been extracting from the Figure 17, has been presented in Table 4. This range of milling parameters indicated the safe zone where, Chatter in minimal having higher MRR.

6.3.   Confirmation Test

The main aim of this work is to obtain optimal parameters which will give minimal chatter at optimal MRR. It is well known facts that whenever chatter minimizes, MRR also diminishes. In experimental section, CI and MRR has been calculated for the 27 experiments and it has been found that for experimental number 27, the value of CI and MRR are 3.158 and 3.69, respectively. These values are highest values among all the 27 experimental runs.

However, in order to aforementioned objective, optimal milling parameters have been ascertained using ANN based prediction models. Based on ascertained optimal milling parameters, a range has been selected and validation experiment has been conducted, as presented in Table 5. After performing the validation experiment, CI and MRR have been calculated. It has been found out that the value of CI and MRR are 1.46 and 3.11, respectively.

In order to validate the optimal parameters, these values are compared with highest value of CI and MRR viz. 3.158 and 3.69, respectively. After comparing it has been found out that,

12

the values of CI and MRR for the validation experiment, has been decreased by 116.30 % and 18.6 %, respectively. Additionally, the CI value for the validation test fell below the stability threshold, as illustrated in Figure 13. Examining the surface texture confirmed the accuracy of the developed parameter range. Consequently, the proposed method proves effective in determining stable milling parameters that lead to higher MRR and improved surface finish. In summary, the derived milling parameters position themselves within a stable machining zone, resulting in enhanced MRR.

7.   Conclusion

The two major goals of this study are to diagnose chatter beginning at the early stages and to determine the setting a realistic of control factors to use during milling operations in order to achieve a high-quality surface and greater MRR. A novel LMD method based on cubic spline interpolation has been employed to accomplish the first goal. Later, ANN models for the responses viz. CI and MRR were designed to accomplish the goal. Results from the verification test indicate that, the ascertained range of milling parameters is able to generate a best surface finish and a better MRR.

References

1.   Muhammad, R., Ahmed, N., Maqsood, S. *et al.,* "Influence of tool material on forces, temperature, and surface quality of Ti-15333 alloy in CT and UAT", *Sci. Iran.*, **26**(5), pp. 2805–2816 (2019).

2.   Tao, J., Qin, C., Xiao, D. *et al.,* "Timely chatter identification for robotic drilling using a local maximum synchrosqueezing-based method", *J. Intell. Manuf.*, **31**(5), pp. 1243–1255 (2020).

3.   Tran, M. Q., Liu, M. K., and Elsisi, M., "Effective multi-sensor data fusion for chatter detection in milling process", *ISA Trans.*, **125**, pp. 514–527 (2022).

4.   Cuka, B. and Kim, D. W., "Fuzzy logic based tool condition monitoring for end-milling", *Robot. Comput. Integr. Manuf.*, **47**(December), pp. 22–36 (2017).

5.   Mishra, R. and Singh, B., "SBLMD–ANN–MOPSO-based hybrid approach for determining optimum parameter in CNC milling", *Soft Comput.*, **27**(11), pp. 7299–7320 (2023).

6.   Daldal, N., Cömert, Z., and Polat, K., "Automatic determination of digital modulation

types with different noises using Convolutional Neural Network based on time–frequency information", *Appl. Soft Comput. J.*, **86**, p. 105834 (2020).

7. Tran, M. Q., Liu, M. K., and Tran, Q. V., "Milling chatter detection using scalogram and deep convolutional neural network", *Int. J. Adv. Manuf. Technol.*, **107**(3–4), pp. 1505–1516 (2020).

8. Noori, M., Wang, H., Altabey, W. A. *et al.,* "A modified wavelet energy rate-based damage identification method for steel bridges", *Sci. Iran.*, **25**(6B), pp. 3210–3230 (2018).

9. Yoon, M. C. and Chin, D. H., "Cutting force monitoring in the endmilling operation for chatter detection", *Proc. Inst. Mech. Eng. Part B J. Eng. Manuf.*, **219**(6), pp. 455–465 (2005).

10. Cai, K., Cao, W., Aarniovuori, L. *et al.,* "Classification of Power Quality Disturbances Using Wigner-Ville Distribution and Deep Convolutional Neural Networks", *IEEE Access*, **7**, pp. 119099–119109 (2019).

11. Shrivastava, Y. and Singh, B., "Estimation of stable cutting zone in turning based on empirical mode decomposition and statistical approach", *J. Brazilian Soc. Mech. Sci. Eng.*, **40**(2) (2018).

12. Zhang, Q., Tu, X., Li, F. *et al.,* "An effective chatter detection method in milling process using morphological empirical wavelet transform", *IEEE Trans. Instrum. Meas.*, **69**(8), pp. 5546–5555 (2020).

13. Zhang, Z., Li, H., Meng, G. *et al.,* "Chatter detection in milling process based on the energy entropy of VMD and WPD", *Int. J. Mach. Tools Manuf.*, **108**, pp. 106–112 (2016).

14. Liu, J., Wu, B., Wang, Y. *et al.,* "An integrated condition-monitoring method for a milling process using reduced decomposition features", *Meas. Sci. Technol.*, **28**(8), p. 085101 (2017).

15. Liu, Y., Wang, X., Lin, J. *et al.,* "Correlation analysis of motor current and chatter vibration in grinding using complex continuous wavelet coherence", *Meas. Sci. Technol.*, **27**(11), p. 115106 (2016).

16. Ji, Y., Wang, X., Liu, Z. *et al.,* "Early milling chatter identification by improved empirical mode decomposition and multi-indicator synthetic evaluation", *J. Sound*

Vib., **433**, pp. 138–159 (2018).

17. Li, Z., Chen, J., Zi, Y. *et al.,* "Independence-oriented VMD to identify fault feature for wheel set bearing fault diagnosis of high speed locomotive", *Mech. Syst. Signal Process.*, **85**, pp. 512–529 (2017).

18. Smith, J. S., "The local mean decomposition and its application to EEG perception data", *J R Soc Interface*, **2**(5), pp. 443–454 (2005).

19. Mishra, R. and Singh, B., "Stability analysis in milling process using spline based local mean decomposition (SBLMD) technique and statistical indicators", *Meas. J. Int. Meas. Confed.*, **174**, p. 108999 (2021).

20. Mishra, R. and Singh, B., "Extenuating Chatter Vibration in Milling Process Using a New Ensemble Approach", *J. Vib. Eng. Technol.*, **10**(4), pp. 1235–1252 (2022).

21. Vazirizade, S. M., Bakhshi, A., and Bahar, O., "Online nonlinear structural damage detection using Hilbert Huang transform and artificial neural networks", *Sci. Iran.*, **26**(3A), pp. 1266–1279 (2019).

22. Devillez, A. and Dudzinski, D., "Tool vibration detection with eddy current sensors in machining process and computation of stability lobes using fuzzy classifiers", *Mech. Syst. Signal Process.*, **21**(1), pp. 441–456 (2007).

23. Chen, G. S. and Zheng, Q. Z., "Online chatter detection of the end milling based on wavelet packet transform and support vector machine recursive feature elimination", *Int. J. Adv. Manuf. Technol.*, **95**(1–4), pp. 775–784 (2018).

24. Mishra, R., Gupta, P., and Singh, B., "An intelligent approach to extract chatter and metal removal rate features impromptu from milling sound signal", *Proc. Inst. Mech. Eng. Part E J. Process Mech. Eng.* (2023).

25. Mohanraj, T. and Tamilvanan, A., "Decision support system for tool condition monitoring in milling process using artificial neural network", *J. Eng. Res.*, **10**(4), pp. 142–155 (2022).

26. Shaul Hameed, S., Muralidharan, V., and Ane, B. K., "Comparative analysis of fuzzy classifier and ANN with histogram features for defect detection and classification in planetary gearbox", *Appl. Soft Comput.*, **106**, p. 107306 (2021).

27. Yanis, M., Mohruni, A. S., Sharif, S. *et al.,* "Application of RSM and ANN in

Predicting Surface Roughness for Side Milling Process under Environmentally Friendly Cutting Fluid", *J. Phys. Conf. Ser.*, **1198**(4), p. 042016 (2019).

28. Jena, S. P. and Parhi, D. R., "Fault detection in cracked structures under moving load through a recurrent-neural-networks-based approach", *Sci. Iran.*, **27**(4), pp. 1886–1896 (2020).

29. Salimiasl, A., Erdem, A., and Rafighi, M., "Applying a multi-sensor system to predict and simulate the tool wear using articial neural networks", *Sci. Iran.*, **24**(6), pp. 2864–2874 (2017).

30. Altintaş, Y. and Budak, E., "Analytical Prediction of Stability Lobes in Milling", *CIRP Ann. - Manuf. Technol.*, **44**(1), pp. 357–362 (1995)

List of Figures

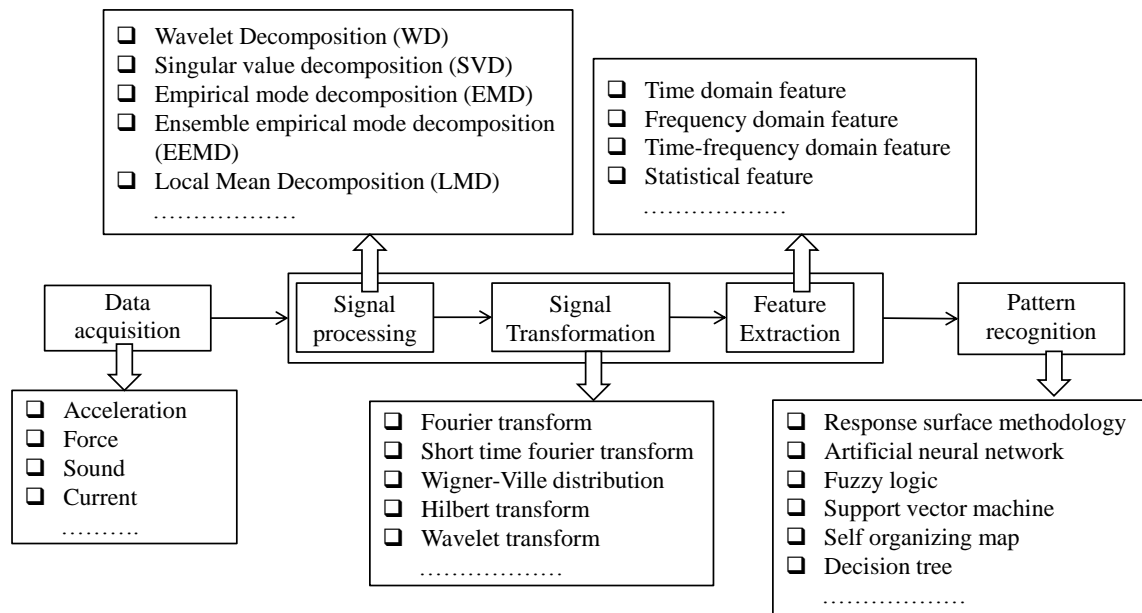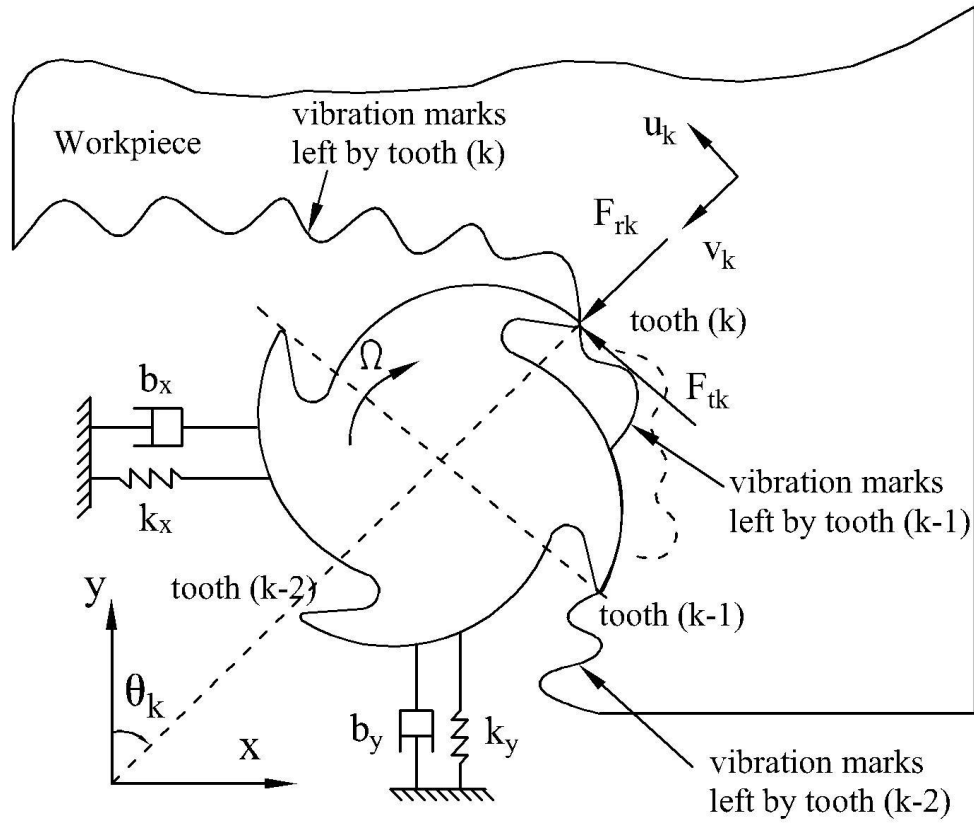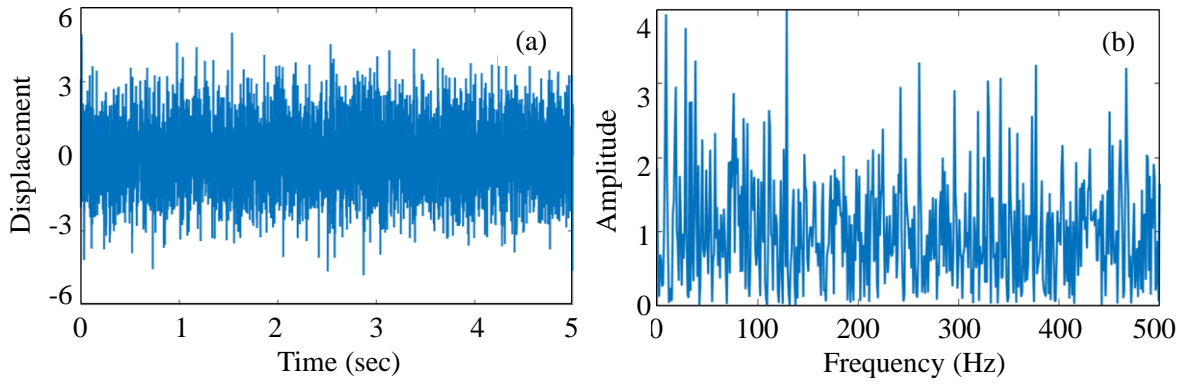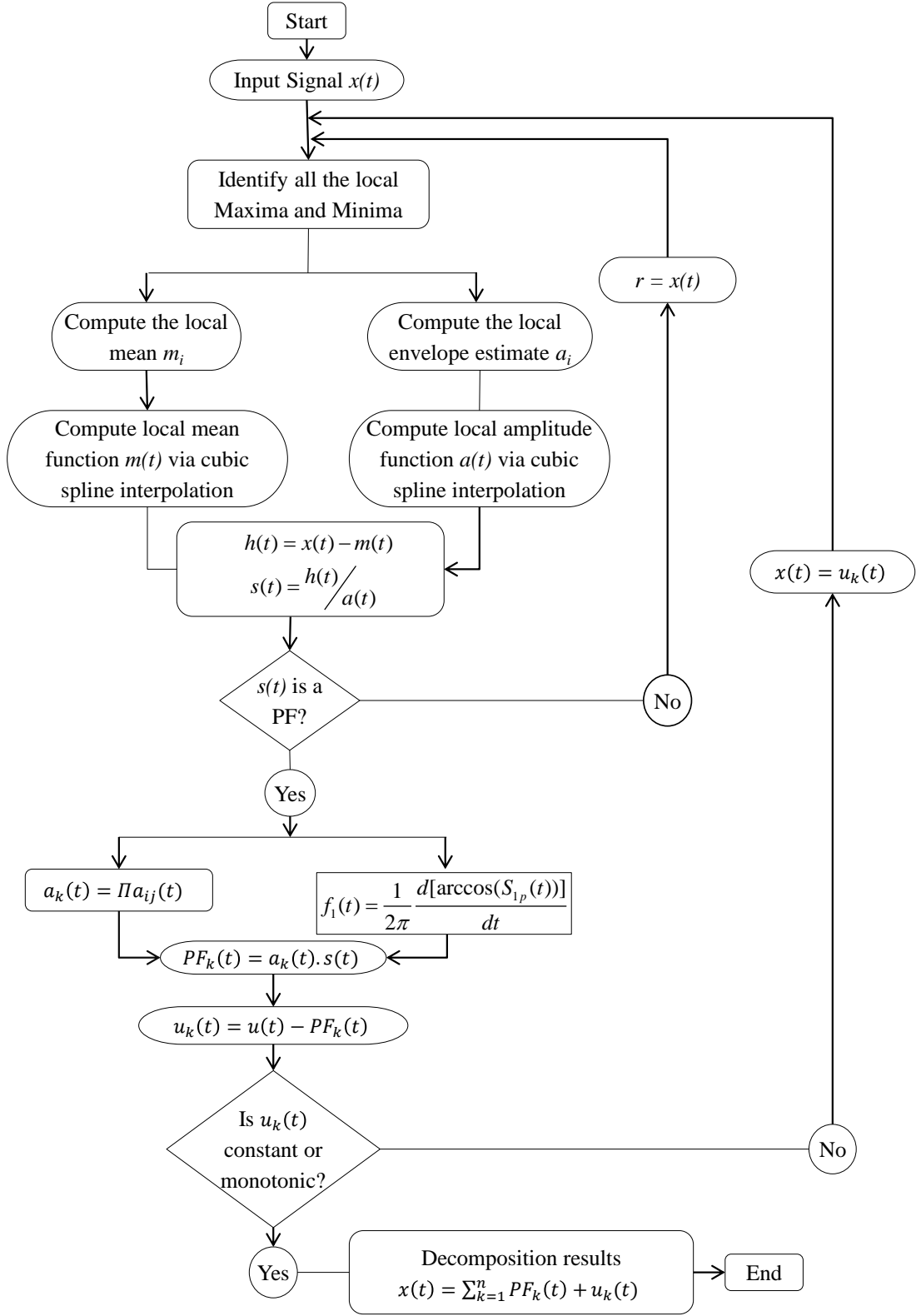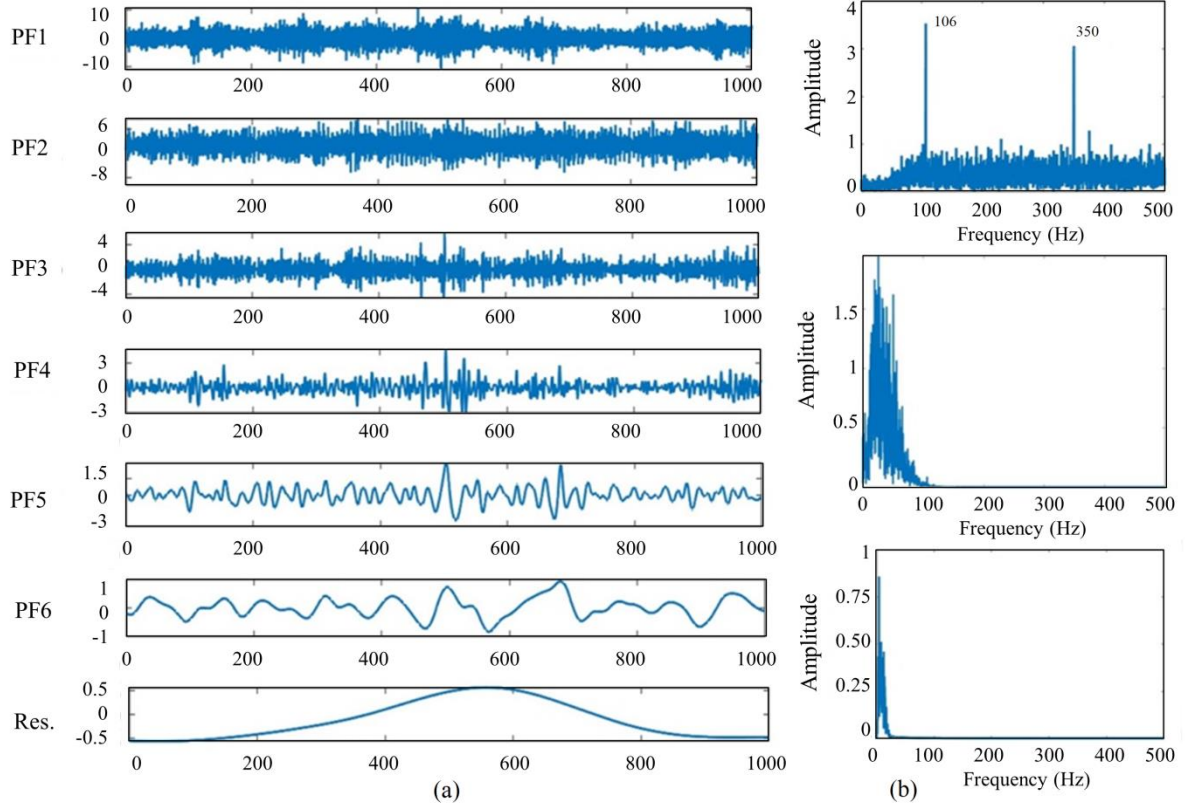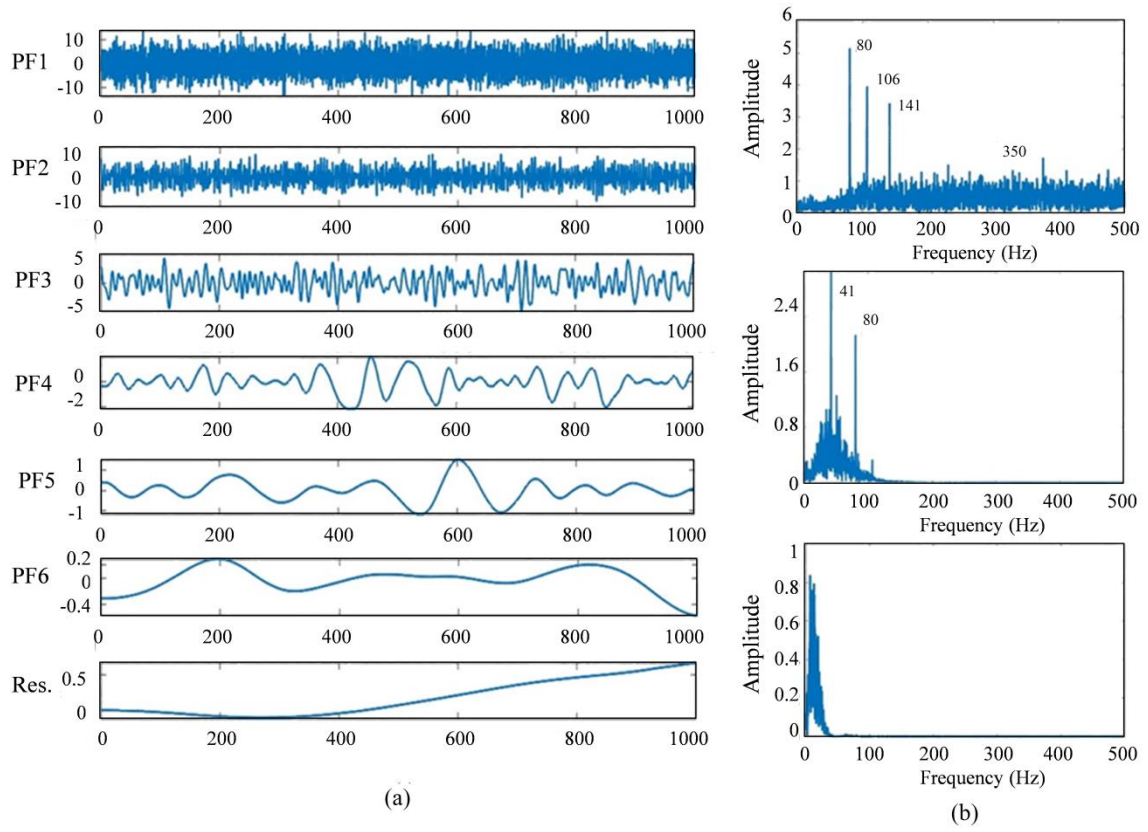| Figure No.	Figure Caption
Figure 1	Steps in chatter diagnosis
Figure 2	Spring mass model milling system
Figure 3	(a) Simulated signal in time domain, and (b) Simulated signal in frequency domain
Figure 4	Algorithm used in SBLMD
Figure 5	(a) PF using C-LMD, and (b) first three PF's FFT
Figure 6	(a) PF using SBLMD, and (b) first three PF's FFT
Figure 7	Set-up of microphone during experimentation
Figure 8	Acquired milling signal using microphone
Figure 9	The fluctuation in MRR values for all 27 experimental runs
Figure 10	PF's extracted using SBLMD of real milling signal
Figure 11	(a) CC and (b) NER
Figure 12	Frequency peaks of the reconstructed milling signal
Figure 13	The fluctuation in CI values for all 27 experimental runs
Figure 14	ANN Model
Figure 15	MRR error in TANSIG, LOGSIG and PURELIN
Figure 16	CI error in TANSIG, LOGSIG and PURELIN
Figure 17	Contours plots for MRR and CI

List of Tables

Table No.	Table Caption
Table 1	Milling parameters with their levels
Table 2	Absolute percentage deviation for TANSIG, LOGSIG and PURELIN
Table 3	Suitable ranges for responses
Table 4	Safe ranges for input milling parameters
Table 5	Validation test

Figure 1 Steps in chatter diagnosis

Figure 2 Spring mass model milling system

Figure 3 (a) Simulated signal in time domain, and **(b)** Simulated signal in frequency domain

Figure 4 Algorithm used in SBLMD

20

Figure 5 (a) PF using C-LMD, and **(b)** first three PF's FFT

Figure 6 (a) PF using SBLMD, and **(b)** first three PF's FFT
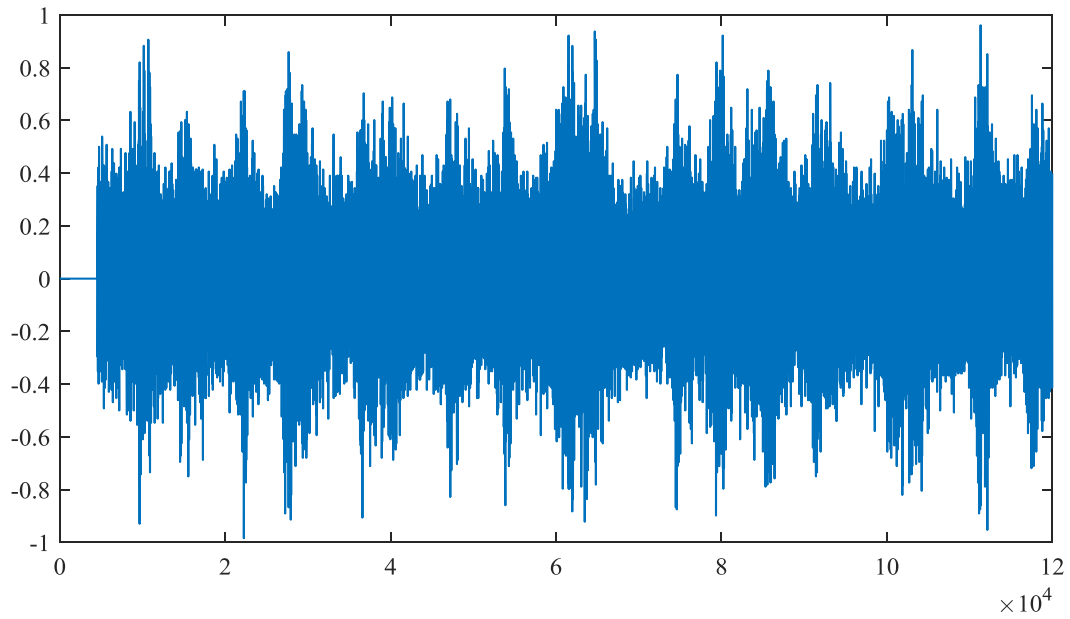

Figure 7 Set-up of microphone during experimentation
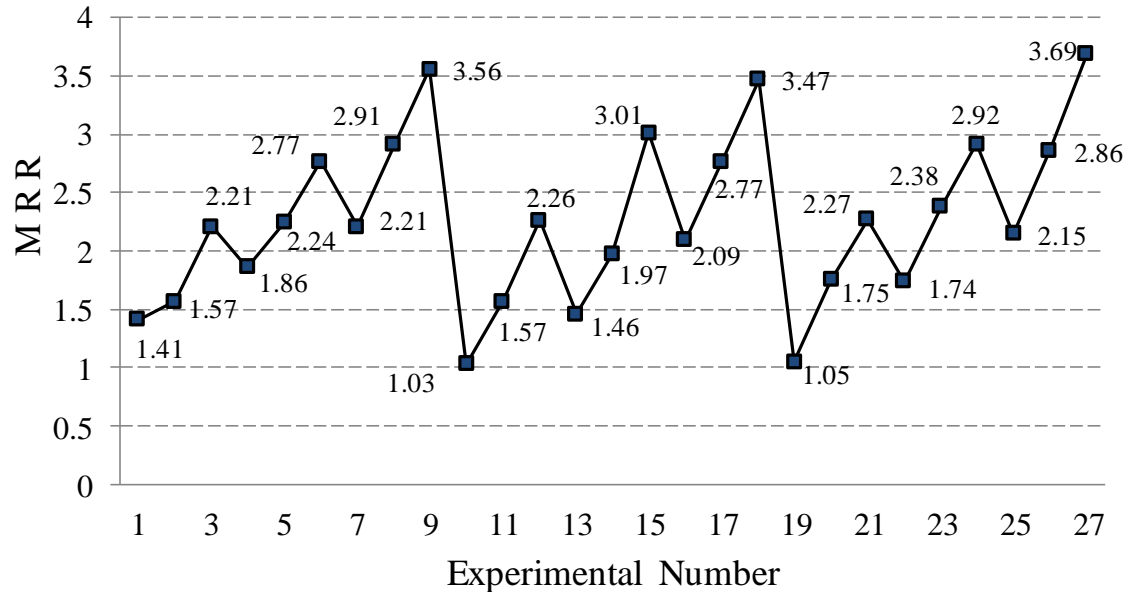

Figure 8 Acquired milling signal using microphone

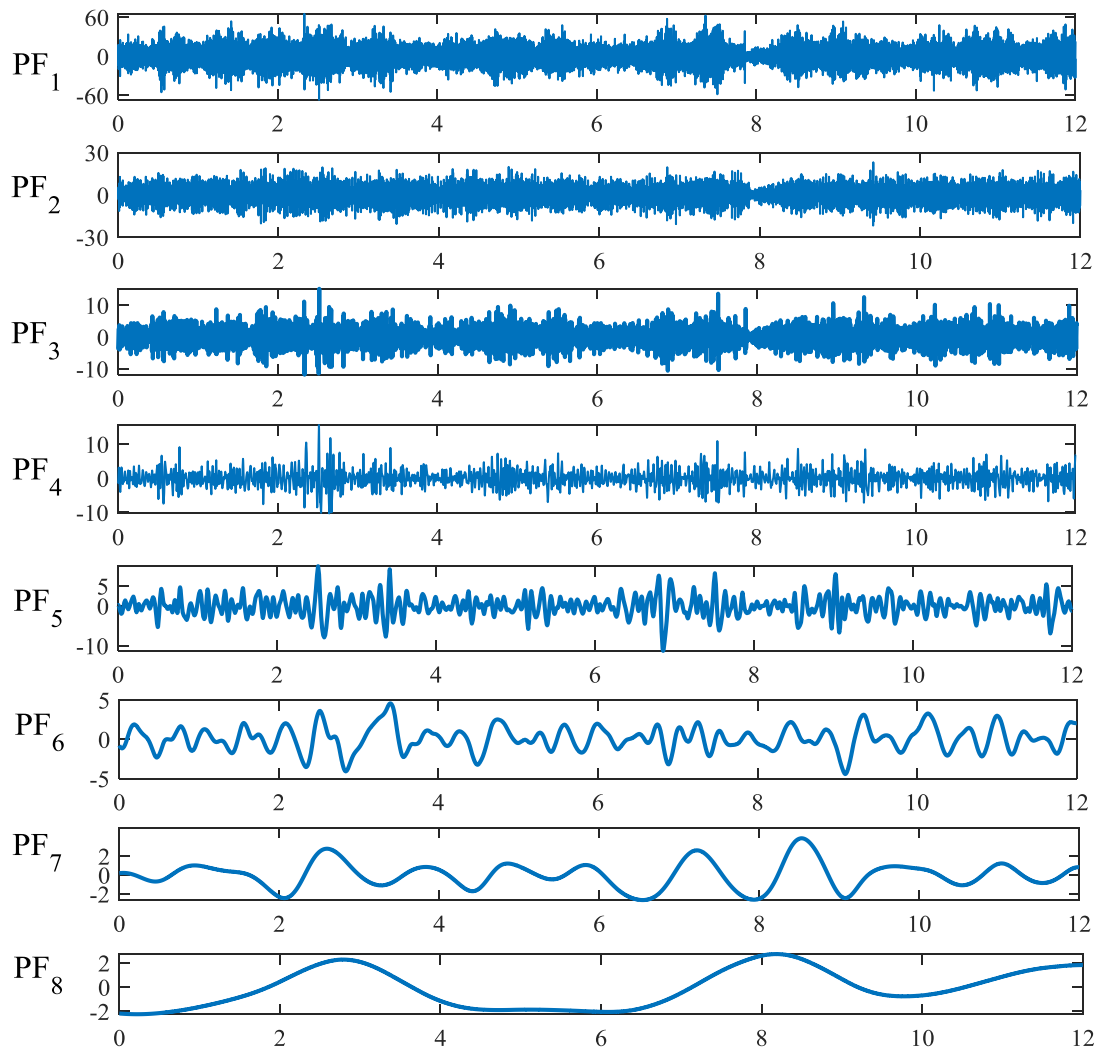**Figure 9** The fluctuation in MRR values for all 27 experimental runs

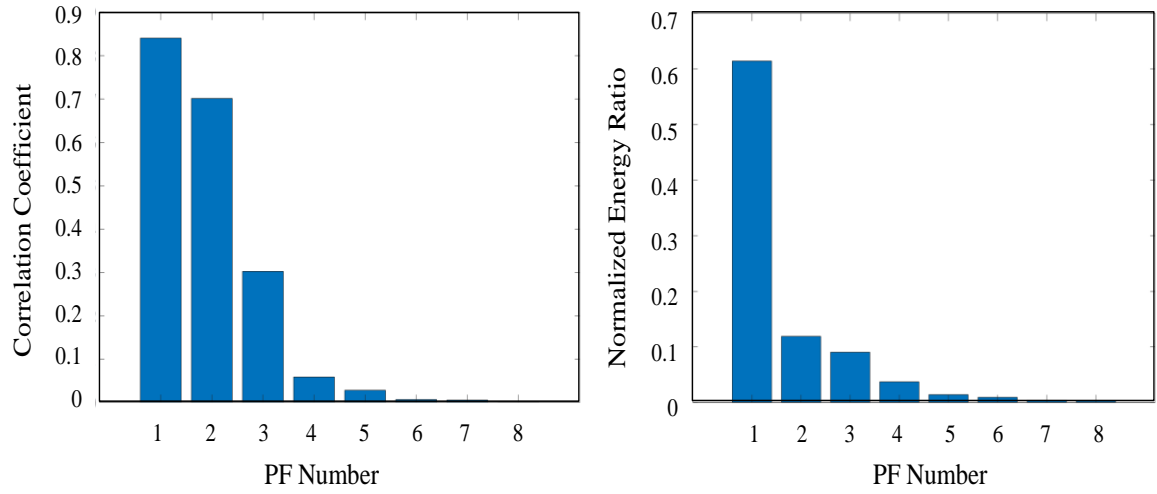**Figure 10** PF's extracted using SBLMD of real milling signal

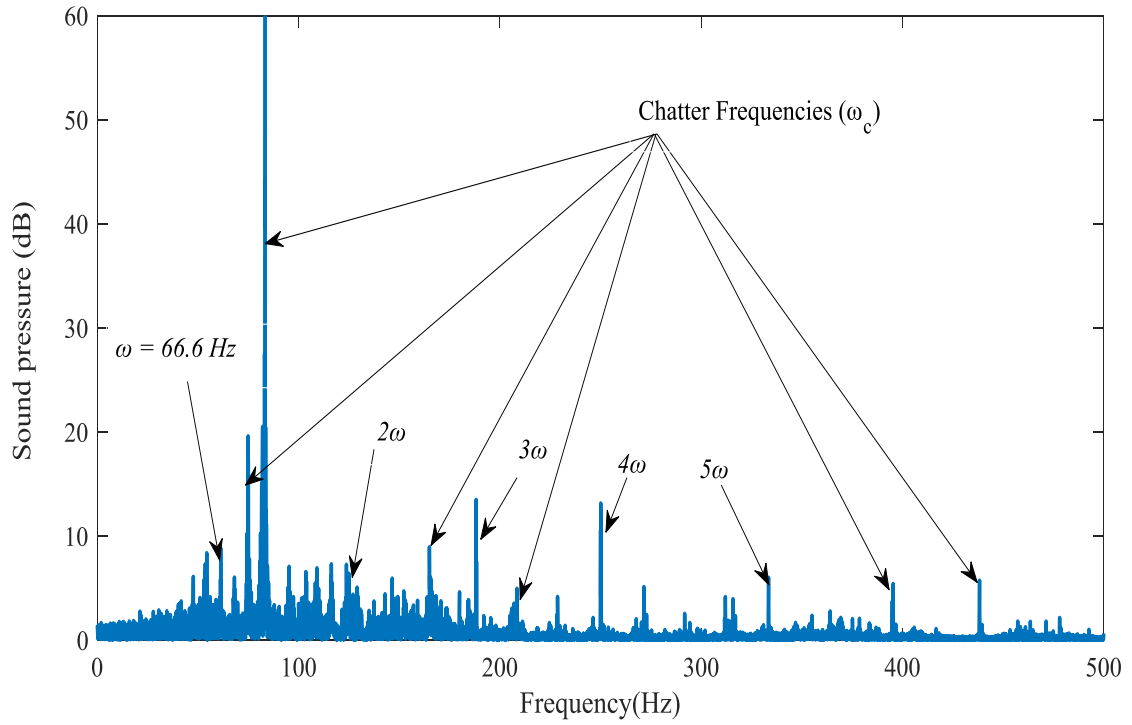23

Figure 11 (a) CC and **(b)** NER

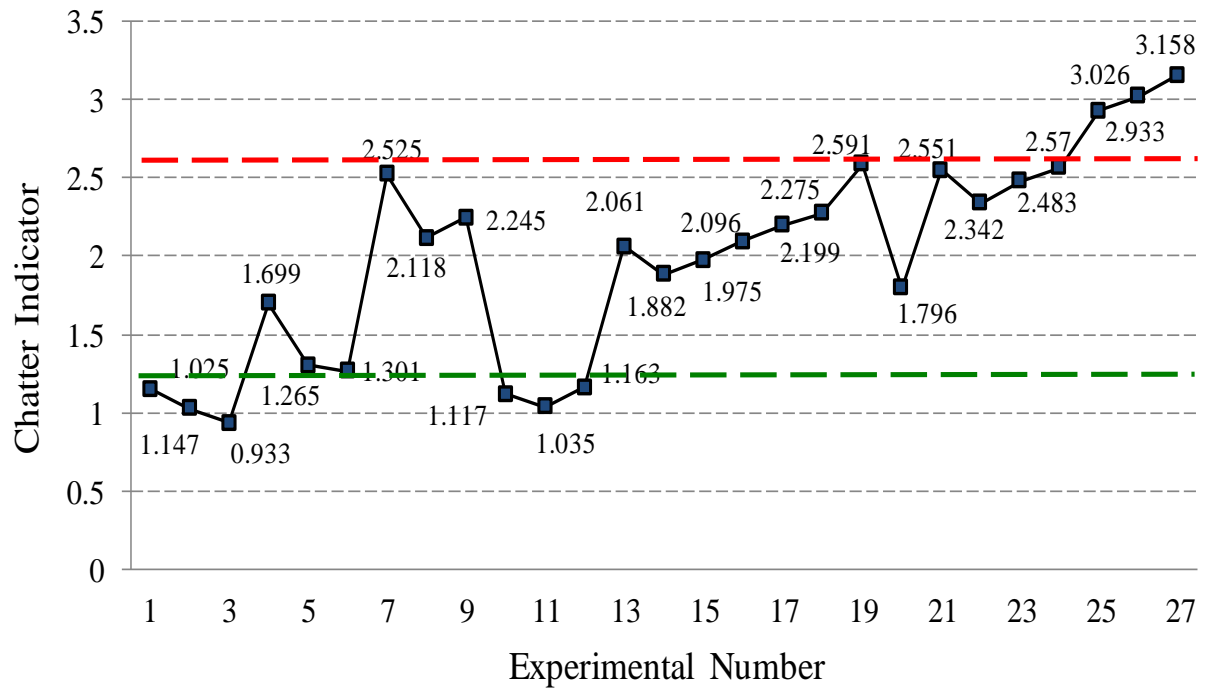**Figure 12** Frequency peaks of the reconstructed milling signal

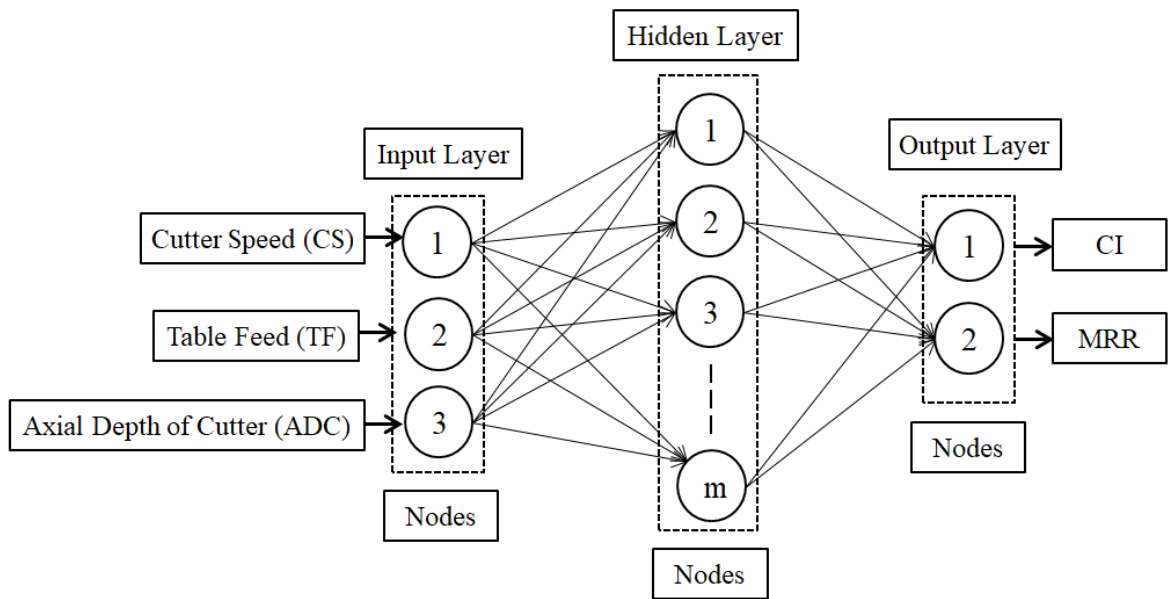**Figure 13** The fluctuation in CI values for all 27 experimental runs
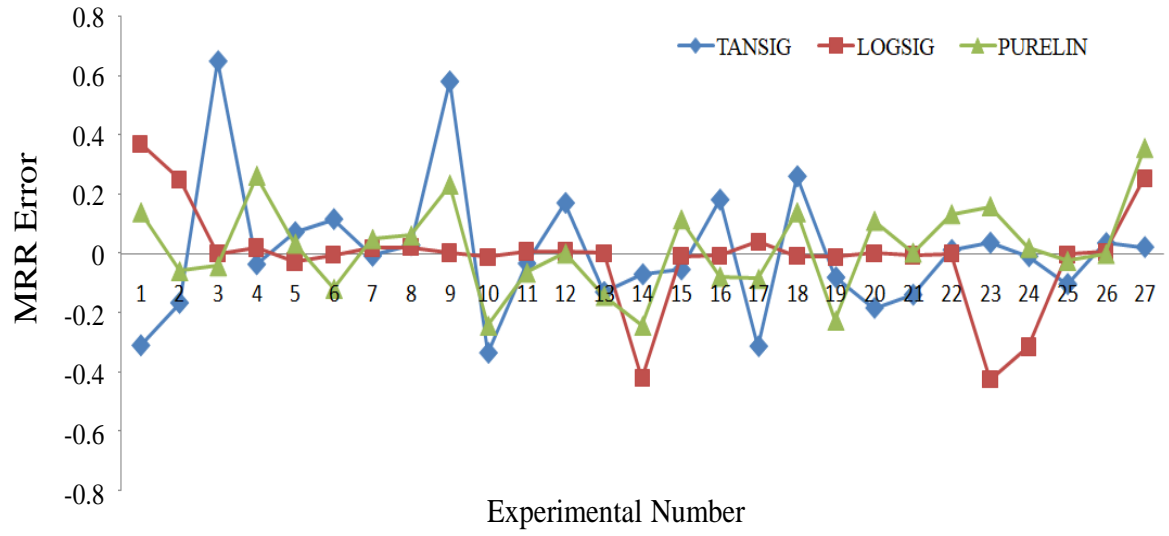

Figure 14 ANN Model
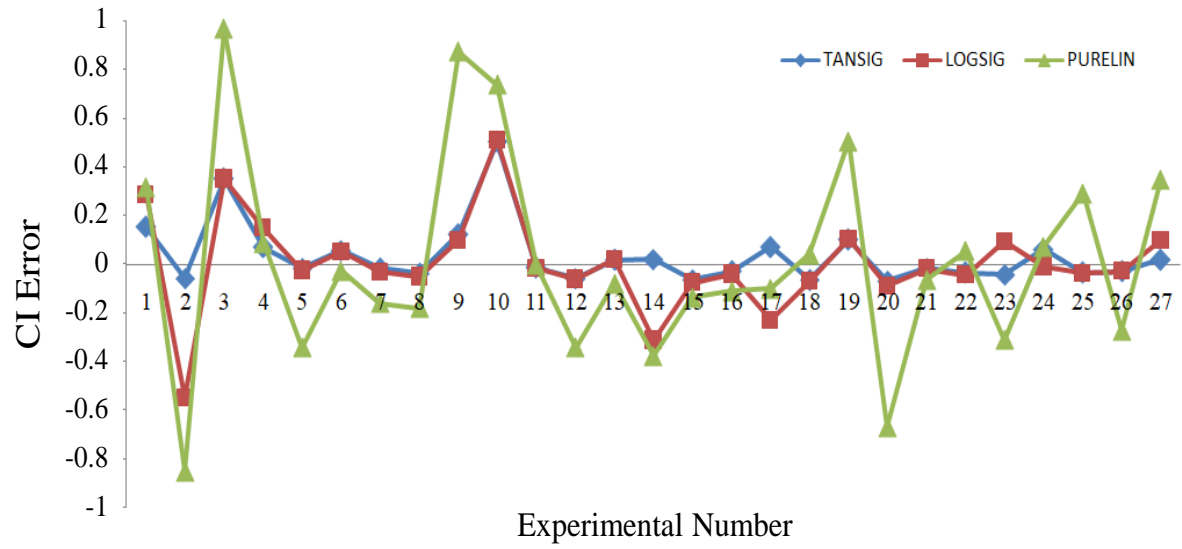
Figure 15 MRR errors in TANSIG, LOGSIG and PURELIN

Figure 16 CI errors in TANSIG, LOGSIG and PURELIN

26

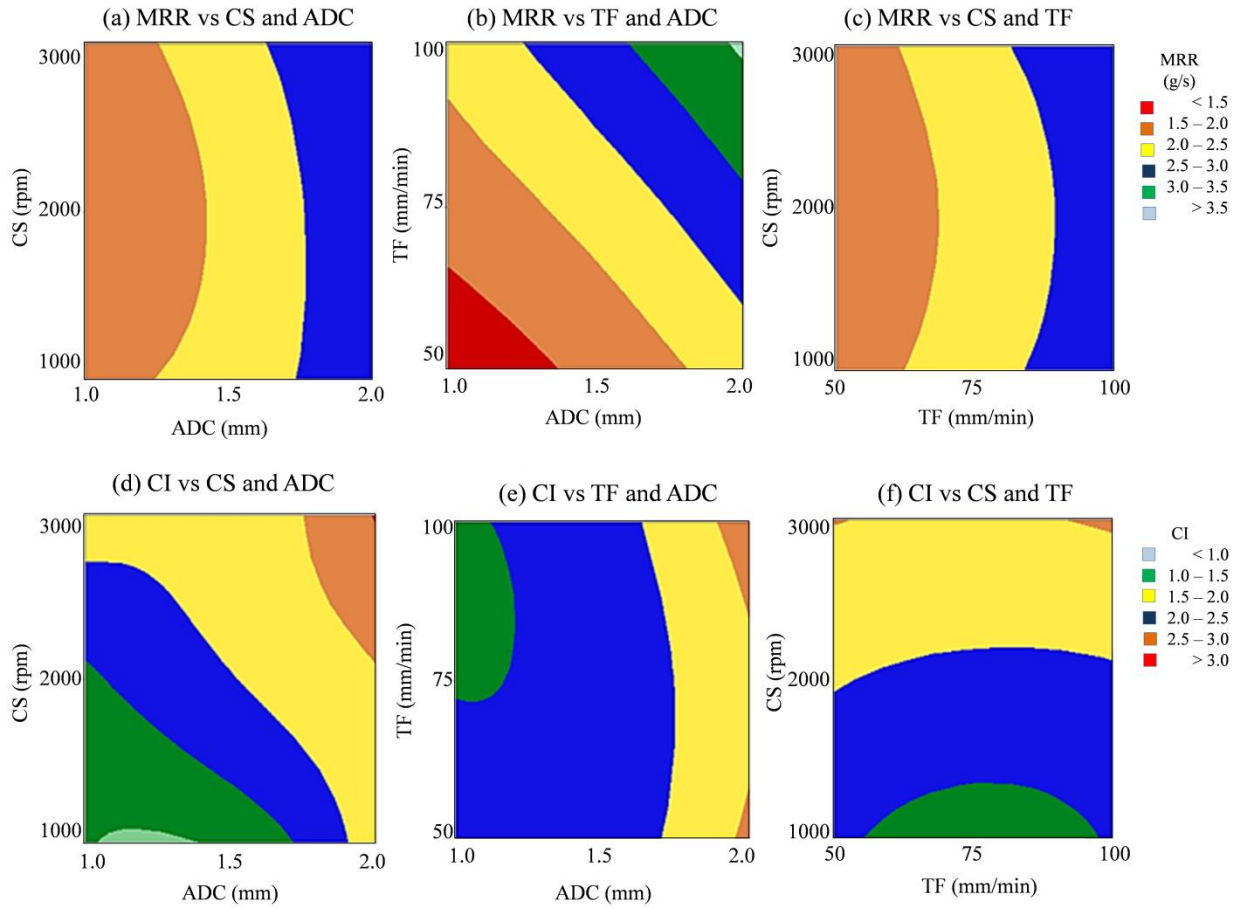**Figure 17** Contours plots for MRR and CI

Table 1 Milling parameters with their levels

Parameters \ level	1	2	3
Table feed (TF)	50 *mm/min*	75 *mm/min*	100 *mm/min*
Cutter speed (CS)	1000 *rpm*	2000 *rpm*	3000 *rpm*
Axial depth of cutter (ADC)	1 *mm*	1.5 *mm*	2 *mm*

Table 2 Absolute percentage deviation for TANSIG, LOGSIG and PURELIN

Exp. No.	TANSIG		LOGSIG		PURELIN	
	MRR	**CI**	**MRR**	**CI**	**MRR**	**CI**
1	22.005	13.389	35.595	13.326	11.017	2.877
2	10.592	4.996	18.901	30.577	3.581	21.326
3	29.440	13.645	0.018	0.012	1.835	31.168
4	1.943	6.866	1.079	8.470	16.505	5.680

5	3.233	1.419	1.196	0.880	1.575	23.488
6	4.216	3.273	0.147	0.369	4.076	4.151
7	0.315	1.658	0.863	1.561	2.335	12.134
8	0.972	3.162	0.756	1.036	2.178	10.054
9	16.351	4.928	0.091	1.017	7.023	43.777
10	32.578	29.707	1.141	0.495	19.054	15.363
11	2.105	0.566	0.439	0.175	3.878	0.596
12	7.587	2.413	0.347	0.108	0.068	10.754
13	8.888	1.539	0.139	0.206	8.826	7.079
14	3.544	1.195	17.645	15.041	10.955	3.268
15	1.787	2.506	0.264	0.461	4.017	2.410
16	8.725	2.265	0.348	0.733	3.536	5.269
17	11.308	3.720	1.476	13.248	2.950	7.094
18	7.539	2.449	0.240	0.235	4.211	4.524
19	7.650	4.097	1.127	0.082	17.637	19.002
20	10.486	3.154	0.121	1.050	6.812	21.645
21	6.124	0.502	0.238	0.059	0.193	1.501
22	0.727	1.608	0.010	0.391	8.330	4.905
23	1.544	1.815	15.131	6.475	7.233	15.477
24	0.305	2.103	9.740	2.321	0.698	2.766
25	4.773	1.455	0.100	0.126	1.088	17.171
26	1.243	1.284	0.188	0.114	0.013	9.702
27	0.604	0.663	7.422	2.542	10.707	8.687
AAPD	**7.651**	**4.310**	**4.250**	**3.745**	**5.938**	**11.551**

Table 3 Suitable ranges for responses

Group	CI	MRR
Satisfactory	CI ≥ 2.56	MRR ≤ 1.47
Medium	2.56 > CI > 1.29	1475 < MRR < 2.97
Un-Satisfactory	CI ≤ 1.29	MRR ≥ 2.97

Table 4 Safe ranges for input milling parameters

	Axial depth of cutter	**Table feed rate**	**Cutter Speed**
MRR	1.25 – 2	60 - 100	1000 - 3000
CI	1 – 1.8	50 - 100	1000 - 2300
Safe Range	1.25 – 1.8	60 – 100	1000 - 2300

Table 5 validation test

Exp. No.	ADC	CS	TF	CI	MRR	Surface view
1.	1.7	1600	99	1.46	3.11	

Brief Technical Biography

***Rohit Mishra*:** Rohit Mishra is a faculty member in the Department of Mechanical Engineering. He earned his B.Tech in Mechanical Engineering from Uttar Pradesh Technical University in 2010, followed by his M.Tech from the Indian Institute of Technology, Roorkee in 2012, also in Mechanical Engineering. He holds a Ph.D. in the field, focusing on "Stability Analysis of Milling Operation for Higher Productivity." He has contributed significantly to the academic landscape with the publication of 15 articles indexed in SCI and Scopus, featured in reputable journals. His areas of expertise encompass production engineering, tool condition monitoring, chatter analysis, and the optimization of machining processes.

Bhagat Singh: Bhagat Singh earned his B.Tech in Mechanical Engineering from NIT, Kurukshetra, and went on to attain a Master of Engineering in Machine Design and Vibration Analysis from NIT, Rourkela. His academic journey culminated in the completion of a Ph.D. degree from the same institution, with his dissertation focusing on the "Study of damping in layered and welded beams." With a wealth of 24 years in teaching and research, Dr. Singh boasts a prolific publication record, contributing over 125 articles to esteemed SCI and Scopus indexed journals. His expertise lies in machine design, vibration analysis, as well as the areas of condition monitoring and fault diagnosis of machine structures, along with tool vibration analysis in machining.